European Journal of Histochemistry 2025; volume 69:4426

Placental mesenchymal stem cell exosomes drive macrophage M2 polarization *via* the miR-146a-5p/TRAF6 axis to ameliorate preeclampsia

Xiaoli Liu,[1,2] Ruiyue Li,[1,2] Junjie Sun,[1,2] Yuanpei Yang,[1,2] Lina Hu[3,4,5]

[1]Department of Obstetrics and Gynecology, Women and Children's Hospital of Chongqing Medical University, Chongqing
[2]Department of Obstetrics and Gynecology, Chongqing Health Center for Women and Children, Chongqing
[3]Department of Obstetrics and Gynecology, The Second Affiliated Hospital of Chongqing Medical University, Chongqing
[4]Joint International Research Lab for Reproduction and Development, Ministry of Education, Chongqing.
[5]Reproduction and Stem Cell Therapy Research Center of Chongqing, China

ABSTRACT

The functional state of placental mesenchymal stem cells (PMSCs) plays a critical role in maintaining maternal-fetal interface homeostasis during the pathogenesis of preeclampsia (PE). Given the limitations associated with direct stem cell transplantation, this study aimed to investigate the therapeutic potential of PMSC-derived exosomes and their carried *miR-146a-5p*. Clinical sample analysis revealed a significant downregulation of *mir-146a-5p* in placental tissues from PE patients, accompanied by impaired proliferation, migration, and angiogenic dysfunction of PMSCs. In an *in vitro* model, exosome intervention effectively reversed hypoxia-induced trophoblast cell apoptosis and enhanced migratory capacity. Furthermore, it promoted macrophage polarization towards the anti-inflammatory M2 phenotype and markedly improved the inflammatory cytokine secretion profile. In a PE mouse model, exosome treatment reduced maternal blood pressure and proteinuria levels, alleviated fetal growth restriction, and up-regulated the expression of M2 macrophage markers in placental tissue. Mechanistically, *miR-146a-5p* targeted *TRAF6* to suppress NF-κB pathway activation, an effect that could be reversed by specific inhibitors. This study is the first to demonstrate that PMSC-derived exosomes, *via* the *miR-146a-5p*/TRAF6 axis, concurrently ameliorate trophoblast dysfunction and correct macrophage polarization imbalance. The efficient intercellular delivery of *miR-146a-5p* by exosomes underscores their potential as a novel targeted therapeutic strategy for PE.

Key words: exosomes; preeclampsia; *miR-146a-5p*; macrophage polarization; placental dysfunction.

Correspondence: Lina Hu, Department of Obstetrics and Gynecology, The Second Affiliated Hospital of Chongqing Medical University, Chongqing, 400010, China. E-mail: cqhulina@hospital.cqmu.edu.cn

Contributions: all the authors made a substantive intellectual contribution, read and approved the final version of the manuscript and agreed to be accountable for all aspects of the work.

Conflict of interest: the authors declare no competing interests, and all authors confirm accuracy.

Ethics approval and consent to participate: this study was approved by the Ethics Committee of Chongqing Maternal and Child Health Care Hospital (Approval No. 2022-010-02). Informed consent was obtained from all of the participants recruited into this study, which was carried out in accordance with the World Medical Association Declaration of Helsinki.

Availability of data and materials: data generated in this study are available upon reasonable request from the corresponding author.

Funding: this work was financially supported by the Natural Science Foundation of Chongqing (Grant No. cstc2021jcyj-msxmX0907).

Introduction

Preeclampsia (PE) is a pregnancy-specific syndrome characterized by new-onset hypertension and proteinuria after 20 weeks of gestation, affecting 3-5% of pregnancies worldwide and leading to severe complications such as maternal organ damage and fetal growth restriction.[1] The core pathological mechanism involves placental dysfunction, which triggers a systemic inflammatory response and vascular endothelial injury in the mother.[2] As key regulators of the placental immune microenvironment, macrophages maintain tissue homeostasis by dynamically switching between pro-inflammatory and anti-inflammatory polarization states, thereby balancing immune responses.[3] Evidence indicates that imbalance in placental macrophage polarization is closely associated with PE pathogenesis.[4,5] This disrupted immune microenvironment exacerbates placental tissue damage through the release of inflammatory factors.

In recent years, mesenchymal stem cell (MSC)-based therapies have demonstrated considerable potential due to their immunomodulatory and tissue regenerative capacities.[6] Particularly, placental mesenchymal stem cells (PMSCs), owing to their unique origin at the maternal-fetal interface and absence of ethical concerns, have emerged as an ideal candidate for cellular therapy in PE.[7] However, challenges such as immune rejection and potential tumorigenic risks associated with direct stem cell transplantation have prompted a shift toward cell-free therapeutic strategies. Among these, exosomes -natural effector vehicles derived from stem cells- have garnered significant attention.[8,9] Exosomes are extracellular vesicles ranging from 30 to 150 nm in diameter, which are released upon the fusion of multivesicular bodies with the plasma membrane. They carry bioactive molecules including proteins, nucleic acids, and lipids, and play a pivotal role in mediating intercellular communication.[10,11] PMSC-derived exosomes exhibit low immunogenicity and favorable tissue penetrability, enabling them to modulate recipient cell functions *via* paracrine signaling pathways.[7] Accumulating evidence indicates that exosomes can deliver nucleic acids such as microRNAs (miRNAs) to regulate target gene expression. The vesicular encapsulation mechanism effectively protects miRNAs from degradation by RNases, while surface adhesion proteins facilitate cell-specific targeting and delivery.[12] In the context of PE, exosomes have been identified as potential biomarkers for predicting disease progression, offering valuable insights for early warning and pathological monitoring.[13] Nevertheless, the precise molecular mechanisms through which exosomes modulate the placental microenvironment remain to be fully elucidated.

miRNAs are a class of approximately 22-nucleotide non-coding RNAs that mediate post-transcriptional gene regulation by targeting messenger RNAs (mRNAs). In the search for biomarkers of PE, placental miRNAs have emerged as key regulatory molecules.[14] For instance, *miR-30b-5p* and *miR-210* have been reported to participate in placental hypoxia response and inflammatory processes.[15,16] Notably, *miR-146a-5p*, which is encoded by the *MIR146A* gene located on human chromosome 5q33.3 and has a mature sequence of 5'-UGAGAACUGAAUUCCAUGGGUU-3', is highly conserved throughout evolution, indicating critical biological functions. Functioning as a key negative regulator of immune and inflammatory responses, *miR-146a-5p* primarily exerts fine-tuned negative feedback on the NF-κB signaling pathway by targeting signaling adaptor proteins such as TNF receptor-associated factor 6 (TRAF6) and interleukin-1 receptor-associated kinase 1 (IRAK1), thereby playing a central role in maintaining immune homeostasis.[17] The roles of *miR-146a-5p* have been extensively investigated in various disease contexts. In the skeletal muscle system, it helps inhibit apoptosis and reactive oxygen species (ROS) production while promoting myofiber differentiation and delaying aging-related muscle decline by modulating mitophagy.[18] Within the immune system, it regulates macrophage polarization and T-cell function.[19,20] Furthermore, *miR-146a-5p* shows promising potential as a biomarker in cancer research.[21] Nevertheless, despite the growing understanding of its functions in diverse disease mechanisms, the specific regulatory networks and therapeutic potential of *miR-146a-5p* in PE remain significantly unexplored.

Based on this foundation, we hypothesize that exosomes derived from PMSCs may deliver *miR-146a-5p* to regulate the TRAF6/NF-κB signaling pathway, thereby ameliorating the pathological environment of PE. This study aims to investigate whether these exosomes, *via* their carried *miR-146a-5p*, can influence trophoblast cell function, modulate macrophage polarization, and alleviate PE-associated inflammatory responses and vascular dysfunction, ultimately providing a novel cell-free therapeutic strategy and theoretical basis for PE treatment.

Materials and Methods

Isolation and culture of PMSCs from human placental tissues

With approval from the hospital ethics committee and written informed consent obtained from all participants, a total of 30 full-term cesarean placental tissue samples were collected (15 from healthy controls and 15 from PE patients). The baseline characteristics of the study participants are summarized in Table 1. Under sterile conditions, placental tissues were transported to the laboratory and thoroughly rinsed with pre-cooled sterile PBS to remove blood contaminants. Tissue fragments approximately 1 mm^3 in size were obtained from the maternal side of the placenta, avoiding areas near the membranes or infarct zones. These fragments were evenly attached to gelatin-coated culture flasks and maintained stationary for 2 h at 37°C in a 5% CO_2 incubator to facilitate adherence. Complete DMEM/F12 medium (Gibco, Waltham, MA,

Table 1. Baseline characteristics of the study participants.

Characteristic	Control (n=15)	Preeclampsia (n=15)	p
Maternal age (years)	29.5±3.2	30.1±4.0	0.65
Gestational age at delivery (weeks)	38.2±1.1	36.5±1.8	<0.01
Systolic blood pressure (mmHg)	115.3±8.4	158.6±12.7	<0.001
Diastolic blood pressure (mmHg)	72.4±6.8	102.3±9.5	<0.001
Proteinuria (mg/24 h)	85.2±22.1	486.7±135.4	<0.001
Neonatal birth weight (g)	3250±285	2450±320	<0.001

USA) supplemented with 10% fetal bovine serum (FBS; Gibco) and 1% penicillin/streptomycin (HyClone, logan, UT, USA) was then gently added along the flask wall. Regular microscopic observation was conducted throughout the culture process.

Isolation and characterization of exosomes

Exosomes were isolated from the supernatant of healthy control PMSCs after 48 h of culture. The supernatant was subjected to a series of differential centrifugations: initially at 300 × g for 10 min at 4°C to remove cells, followed by 2,000 × g for 20 min to pellet dead cells, and then 1,0000 × g for 30 min to eliminate cellular debris. The resulting supernatant was subsequently filtered through a 0.22 μm pore membrane (Millipore, Burlington, MA, USA) and transferred to ultracentrifuge tubes. Exosomes were pelleted *via* ultracentrifugation (Optima XE; Beckman Coulter, Brea, CA, USA) at 100,000 × g for 70 min at 4°C. The supernatant was discarded, and the pellet was gently resuspended in pre-cooled PBS and subjected to a second round of ultracentrifugation under the same conditions for washing. The final exosome pellet was resuspended in a small volume of PBS and either stored at -80°C or used immediately for characterization. The isolated vesicles were identified as exosomes by characteristic morphological features observed under transmission electron microscopy (JEM-1400Flash; JEOL Ltd., Tokyo, Japan).

Cell culture and treatment

The human chorionic trophoblast cell line HTR-8/SVneo and the human monocytic cell line THP-1 were obtained from Cellverse Co., Ltd. (Shanghai, China). HTR-8/SVneo cells were maintained in RPMI-1640 medium (Gibco) supplemented with 10% fetal bovine serum (FBS, Gibco, USA) and 1% penicillin/streptomycin (HyClone). THP-1 cells were cultured in RPMI-1640 medium containing 10% FBS. All cells were incubated at 37°C under a 5% CO_2 atmosphere. To simulate the pathological environment of PE, HTR-8/SVneo cells were seeded into 6-well plates. Upon reaching 70% confluence, the medium was replaced with serum-free medium, and cells were subjected to hypoxic treatment (1% O_2, 37°C) for 24 h in a tri-gas incubator (Thermo Fisher Scientific, Waltham, MA, USA) to establish a trophoblast cell injury model. For THP-1 cells, M0 macrophages were induced by stimulation with 100 ng/mL PMA (P1585; Sigma-Aldrich, St. Louis, MO, USA) for 24 h. After induction, cells were washed with PBS and cultured in fresh medium for an additional 24 h. Subsequently, M1 polarization was induced by treatment with 100 ng/mL LPS (L4391; Sigma-Aldrich) and 20 ng/mL IFN-γ (300-02; PeproTech, Cranbury, NJ, USA) for 24 h.

Transwell

The transwell chamber with an 8 μm pore polycarbonate membrane (Corning Inc., Corning, NY, USA) was placed into a 24-well plate. The upper chamber was filled with 200 μL of serum-free medium, while the lower chamber received 600 μL of complete medium supplemented with 10% FBS (Gibco) as a chemoattractant. Treated cells were resuspended in serum-free medium, and 200 μL of the cell suspension was seeded into the upper chamber. After incubation for 24 h at 37°C under 5% CO_2, the chamber was carefully removed. Non-migrated cells on the upper surface of the membrane were gently removed using a cotton swab. Cells that had migrated to the lower surface of the membrane were fixed with 4% paraformaldehyde at room temperature for 15 min and stained with 0.1% crystal violet solution (Sigma-Aldrich) for 20 min. The membrane was then rinsed gently three times with PBS to remove excess dye. After air-drying, the migrated cells were examined and recorded across five randomly selected fields using an inverted microscope (Olympus, Tokyo, Japan) equipped with a 10 × objective (Zeiss, Oberkochen, Germany). The cell migration ability was subsequently quantified by calculating the average number of migrated cells per field from three independent experiments.

Flow cytometry

Cells from the healthy control and PE groups at passages 3-5 in the logarithmic growth phase were collected and washed with pre-cooled PBS. The cell density was adjusted to approximately 1×10^6 cells/mL, and the cell suspension was aliquoted into flow tubes. Subsequently, 5 μL of anti-human monoclonal antibodies (CD90: 328108; CD45: 368512; BioLegend, San Diego, CA, USA) were added, followed by incubation for 30 min on ice under light-protected conditions. After incubation, cells were washed twice with PBS containing 2% FBS (Gibco,) to remove unbound antibodies and finally resuspended in 300 μL PBS for immediate analysis by flow cytometry (Attune NxT; Thermo Fisher Scientific). For each sample, a minimum of 10,000 events were recorded, and the experiment was independently repeated three times (n=3). The positive rate of CD90 and the negative rate of CD45 were evaluated to confirm the MSC characteristics of PMSCs.

Cell apoptosis was assessed using the Annexin V-FITC/PI double staining kit (BD Biosciences, Franklin Lakes, NJ, USA). After treatment, cells were collected and washed with PBS. The cell pellet was resuspended in 1× Annexin V binding buffer, followed by the addition of 5 μL Annexin V-FITC and 5 μL propidium iodide (PI) working solution. The mixture was gently vortexed and incubated at room temperature for 15 min in the dark. After incubation, an appropriate volume of binding buffer was added, and samples were analyzed within 1 h using flow cytometry (Attune NxT; Thermo Fisher Scientific), with a minimum of 10,000 events acquired per condition.

Cells were harvested and washed twice with PBS, and the cell density was adjusted. The cell suspension was aliquoted into flow tubes and incubated with 5 μL of anti-human monoclonal antibodies (CD86: 305406; CD206: 321110; BioLegend) for 30 min on ice in the dark. Unbound antibodies were removed by washing, and cells were resuspended in PBS for immediate flow cytometric analysis. The expression levels of CD86 (an M1 marker) and CD206 (an M2 marker) were measured based on the acquisition of 10,000 events per sample. All flow cytometry data presented are from three biologically independent experiments.

CCK-8 assay

Following treatment, cells were seeded into 96-well plates at a density of 5×10^3 cells per well, with six replicate wells allocated for each experimental group alongside blank control wells containing only culture medium. After allowing for cell attachment, the plates were further cultured until the predetermined time points of 24 h, 48 h, and 72 h. At each time point, 10 μL of CCK-8 reagent (Beyotime Biotechnology, Haimen, China) was added to each well, followed by incubation at 37°C in the dark for 2 h. The optical density (OD) values were subsequently measured at a wavelength of 450 nm using a microplate reader (BioTek Instruments, Inc., Winooski, VT, USA; Model Synergy H1).

Tube formation

Pre-cooled Matrigel matrix (Corning) was thawed slowly on ice, and 50 μL was evenly coated onto the bottom of a 96-well plate, followed by incubation at 37 °C for 30 min to allow complete polymerization. Treated PMSCs suspended in conditioned medium were seeded onto the surface of the solidified gel at a density of 2×10^4 cells per well, with 100 μL of culture medium added to each well. After the samples were incubated for 24 h at 37°C under 5% CO_2, tubular structures were examined and imaged by capturing

five randomly selected fields per sample using an inverted microscope (Olympus) equipped with a 10 × objective (Zeiss). The angiogenic capacity was subsequently quantified by measuring the total network length, number of branching points, and tube formation area with ImageJ software (NIH, Bethesda, MD, USA). These analyses were performed on images captured from multiple random fields per well across three biologically independent experiments.

ELISA

The concentrations of VEGF, PIGF, sFlt-1, TNF-α, and IL-10 in cell culture supernatants, animal serum, and tissue homogenate supernatants (obtained by homogenizing tissues in RIPA lysis buffer followed by centrifugation at 12,000 × g for 10 min) were quantified using commercial ELISA kits (Enzyme, China). Cell culture supernatants and serum samples were directly assayed, while tissue homogenate supernatants were diluted with PBS to a uniform total protein concentration of 1 mg/mL as determined by BCA assay. All procedures were strictly performed according to the manufacturer's instructions. To ensure the reliability and reproducibility of the data, each sample, including standards, was analyzed in triplicate wells within the same plate, and the entire experiment was independently repeated three times. Briefly, 100 µL of standard or sample was added to each well of antibody-precoated 96-well plates. After incubation with biotinylated detection antibody at 37°C for 60 min and washing, streptavidin-conjugated HRP was added and incubated for 30 min in the dark. Following another washing step, TMB substrate was added and allowed to develop color for 10-15 min under light-protected conditions (exact duration optimized as per kit instructions). The reaction was terminated by adding 2M H_2SO_4, and the optical density (OD) was measured at 450 nm with a reference wavelength of 630 nm.

Fluorescence *in situ* hybridization experiment

Cultured PMSCs on coverslips were fixed with 4% paraformaldehyde at room temperature for 15 min and washed three times with PBS. Permeabilization was performed using 0.2% Triton X-100 at room temperature for 10 min, followed by additional PBS washes. Cells were then digested with proteinase K working solution (20 µg/mL; Sigma-Aldrich) at 37°C for 10 min, and the reaction was terminated by washing with PBS. Prehybridization was carried out with a solution containing 50% formamide (Sigma-Aldrich) in 2×SSC at 42°C for 1 h. A DIG-labeled miR-146a-5p LNA probe (sequence: 5′-CGCCGCTGAGAACTGAATTCC-3′) was diluted to 20 nM in a hybridization buffer containing 40% formamide and 10% dextran sulfate (Sigma-Aldrich), applied to the coverslips, and covered with silanized coverslips. Hybridization was performed overnight at 42 °C in a humidified chamber. The following day, coverslips were washed twice with 2×SSC containing 0.1% Tween-20 (Sigma-Aldrich) for 10 min each, followed by a wash with 0.5×SSC (containing 0.1% Tween-20) at 37°C for 5 min. After blocking with 5% BSA at room temperature for 30 min, an anti-DIG antibody (Roche, 11093274910, diluted 1:500) was applied and incubated at 37°C for 1 h. Following three PBS washes, color development was performed using NBT/BCIP substrate under light-protected conditions for 15 min, with progression monitored microscopically (Olympus). Nuclei were counterstained with hematoxylin for 1 min, and the samples were dehydrated through a graded ethanol series (80%, 95%, and 100%, 2 min each), cleared in xylene for 5 min, and mounted with neutral gum. Finally, slides were observed by examining five randomly selected fields per sample under an inverted fluorescence microscope (Olympus) with a 40 × objective (Zeiss), with positive signals identified as blue-purple cytoplasmic granules. This assessment was consistently confirmed across three independent experimental replicates.

Animal experimentation

Female C57BL/6 mice aged 10–12 weeks were obtained from Jiangsu GemPharmatech Co., Ltd (Jiangsu, China). For mating, one male mouse (12-14 weeks old) was housed with two female mice. The presence of a vaginal plug was designated as gestation day 0 (GD0). Pregnant mice were randomly divided into four groups (n=5 per group): control group, L-NAME group, L-NAME + exosome group, and L-NAME + miR-146a-5p mimic group. All injections and outcome assessments were performed by investigators blinded to the group assignments. From GD10 to GD17, mice in the L-NAME and treatment groups received daily intraperitoneal injections of L-NAME (60 mg/kg/day, HY-18729A, MCE), while the control group received an equal volume of normal saline. Therapeutic interventions began on GD13: the L-NAME + exosome group received PMSC-derived exosomes (100 µg per mouse in 100 µL PBS, administered daily *via* tail vein injection), and the miR-146a-5p mimic group received a chemically synthesized miR-146a-5p mimic (5 nmoL per mouse, RiboBio, China). The control and L-NAME groups were injected with an equal volume of PBS. Systolic blood pressure and 24 h microalbuminuria levels were dynamically monitored throughout the experiment. On GD18, all mice underwent cesarean section to collect fetuses and placentas. Fetal weights were recorded, and all fetal and placental samples were pooled for subsequent analysis without distinction of sex.

RT-qPCR

Total RNA was extracted from animal placental tissues flash-frozen in liquid nitrogen using the TRIzol method (Invitrogen, Waltham, MA, USA). RNA concentration and purity were determined with a NanoDrop 2000 spectrophotometer (Thermo Fisher Scientific), and samples with an A260/A280 ratio ≥1.8 were considered acceptable. Reverse transcription was performed using the PrimeScript™ RT reagent kit (Accurate Biology, Guangzhou, China). Quantitative PCR was carried out on a QuantStudio 5 system (Applied Biosystems, Waltham, MA, USA) with SYBR® Premix Ex Taq™ II (Accurate Biology). GAPDH was used as the reference gene for normalization, and the relative expression levels of target genes (Arg1 and iNOS) were calculated using the $2^{-\Delta\Delta Ct}$ method. All experiments were performed in triplicate to ensure reproducibility. The primer sequences were as follows: *Arg1*-Forward: 5′-CTCCAAGCCAAAGTCCTTAGAG-3′, *Arg1*-Reverse: 5′-AGGAGCTGTCATTAGGGACATC-3′. *iNOS*-Forward: 5′-GTTCTCAGCCCAACAATACAAGA-3′, *iNOS*-Reverse: 5′-GTGGACGGGTCGATGTCAC-3′. *GAPDH*-Forward: 5′-AGGTCGGTGTGAACGGATTTG-3′, *GAPDH*-Reverse: 5′-TGTAGACCATGTAGTTGAGGTCA-3′.

Western blot

Cellular or tissue samples were lysed on ice using pre-cooled RIPA lysis buffer (Beyotime Biotechnology) supplemented with 1% protease inhibitor cocktail for 30 min, followed by centrifugation at 12,000× g for 15 min to collect the supernatant. Protein concentration was determined using the BCA assay (P0012; Beyotime Biotechnology). Subsequently, 30 µg of protein from each sample was mixed with 5× SDS loading buffer and denatured at 95°C for 5 min. The denatured proteins were separated by 10% SDS-PAGE and transferred onto a PVDF membrane (Millipore) *via* the wet transfer method. The membrane was blocked with 5% skim milk (BD Biosciences) at room temperature for 1 h and then incubated overnight at 4°C with the following primary antibodies: CD63 (ab59479, 1:1000; Abcam), TSG101 (ab125011, 1:1000; Abcam), Calnexin (10427-2-AP, 1:2000; Proteintech Tech, Inc., Rosemont, IL, USA), TRAF6 (CST, 8028, 1:1000), p-NF-κB (CST, 3033, 1:1000), NF-κB (CST, 8242, 1:1000), and GAPDH (60004-1-Ig, 1:5000; Proteintech Tech, Inc.). After incubation, the membrane

was washed three times with TBST and probed with corresponding HRP-conjugated secondary antibodies (goat anti-rabbit or anti-mouse, ab205718/ab205719, 1:5000; Abcam) at room temperature for 1 h. Following additional washes, protein bands were visualized using an ECL chemiluminescence reagent (WBKLS0500; Millipore) and analyzed semi-quantitatively by measuring band intensity with ImageJ software, with results expressed as the ratio of target protein to internal reference (GAPDH). All experiments were performed in triplicate to ensure reproducibility.

Dual luciferase reporter assay

The wild-type (WT-TRAF6) and mutant (Mut-TRAF6) dual luciferase reporter plasmids were constructed by Sangon Biotech (China). Cells were seeded into 24-well plates and transfected at approximately 70% confluence using Lipofectamine 3000 (Invitrogen). Each well received a co-transfection mixture containing 500 ng of either WT or Mut reporter plasmid, along with 50 nM miR-146a-5p mimic or negative control mimic (NC mimic). After 48 h of transfection, fluorescence activity was measured using a dual luciferase assay kit (E1910; Promega, Madison, WI, USA) following the manufacturer's protocol. All experiments were performed in triplicate to ensure reproducibility.

Statistical analysis

All experiments were conducted with three technical replicates unless otherwise indicated. Data are expressed as mean ±SD. Statistical analyses were performed using GraphPad Prism 9 software (GraphPad Software, La Jolla, CA, USA), employing Student's *t*-test for two-group comparisons or one-way ANOVA with Tukey's *post-hoc* test for multiple comparisons, as dictated by experimental design. A p-value <0.05 was deemed statistically significant.

Results

Impaired function of PMSCs in PE patients and downregulated expression of miR-146a-5p

PMSCs were successfully isolated from placental tissues of both PE patients and normal pregnancies using the tissue explant adherence method. Flow cytometric analysis confirmed that cells from both groups exhibited characteristic MSC surface markers, with high expression of CD90 and low expression of CD45, and morphologically displayed typical fibroblast-like spindle-shaped cells growing in a whorled pattern (Figure 1 A,B). Functional assessments revealed significant impairments in PE-derived PMSCs, as evidenced by CCK-8 assays showing markedly reduced proliferative capacity (Figure 2A), transwell migration assays demonstrating impaired migratory ability with fewer penetrating cells (Figure 2B), and *in vitro* vasculogenic differentiation assays indicating sparse and disrupted tubular network formation compared to the dense and well-organized structures in controls (Figure 2C). ELISA further indicated significantly decreased secretion of pro-angiogenic factors VEGF and PIGF along with elevated levels of the anti-angiogenic factor sFlt-1 in the conditioned medium of PE-PMSCs (Figure 2D). Fluorescence *in situ* hybridization (FISH) analysis revealed a substantial reduction in *miR-146a-5p* expression in PE-PMSCs (Figure 2E). Collectively, these findings demonstrate that PMSCs from PE patients exhibit functional deficiencies in proliferation, migration, angiogenic differentiation, and paracrine secretion, accompanied by downregulation of *miR-146a-5p*.

PMSCs-derived exosomes ameliorate hypoxia-induced trophoblast injury *via* miR-146a-5p

To investigate the reparative effects of PMSC-derived exosomes on the pathological environment of PE, exosomes were first isolated from the culture supernatant of healthy PMSCs using ultracentrifugation. Transmission electron microscopy revealed typical cup-shaped vesicular structures, and Western blot analysis confirmed strong positive expression of exosomal marker proteins CD63 and TSG101, along with negative expression of the endoplasmic reticulum protein Calnexin (Figure 3A). A functional injury model was established by subjecting HTR-8/SVneo cells to hypoxic conditions for 24 h. Subsequent co-culture with PKH67-labeled PMSCs-derived exosomes or miR-146a-5p mimic significantly enhanced the uptake capacity of exosomes in hypoxia-treated cells (Figure 3B). Semi-quantitative analysis of fluorescence intensity further suggested that hypoxic stress might promote the internalization of exosomes, potentially indicating a stress-dependent uptake mechanism. RT-qPCR analysis demonstrated that

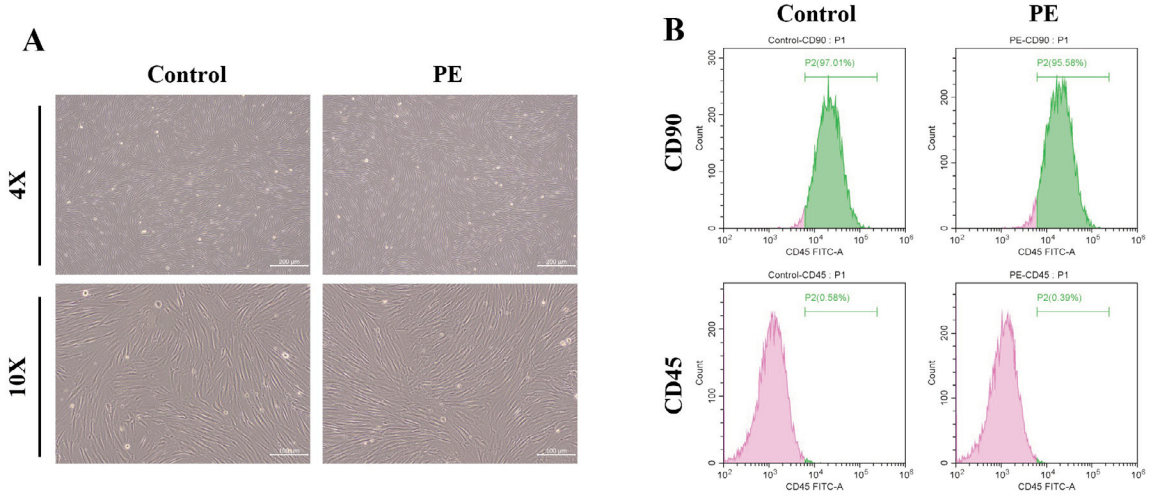

Figure 1. Isolation and identification of PMSCs. **A**) Morphology of PMSCs showing typical fibroblast-like spindle shape; scale bar: 100 µm. **B**) Flow cytometry analysis of MSC surface markers $CD90^{+}/CD45^{-}$.

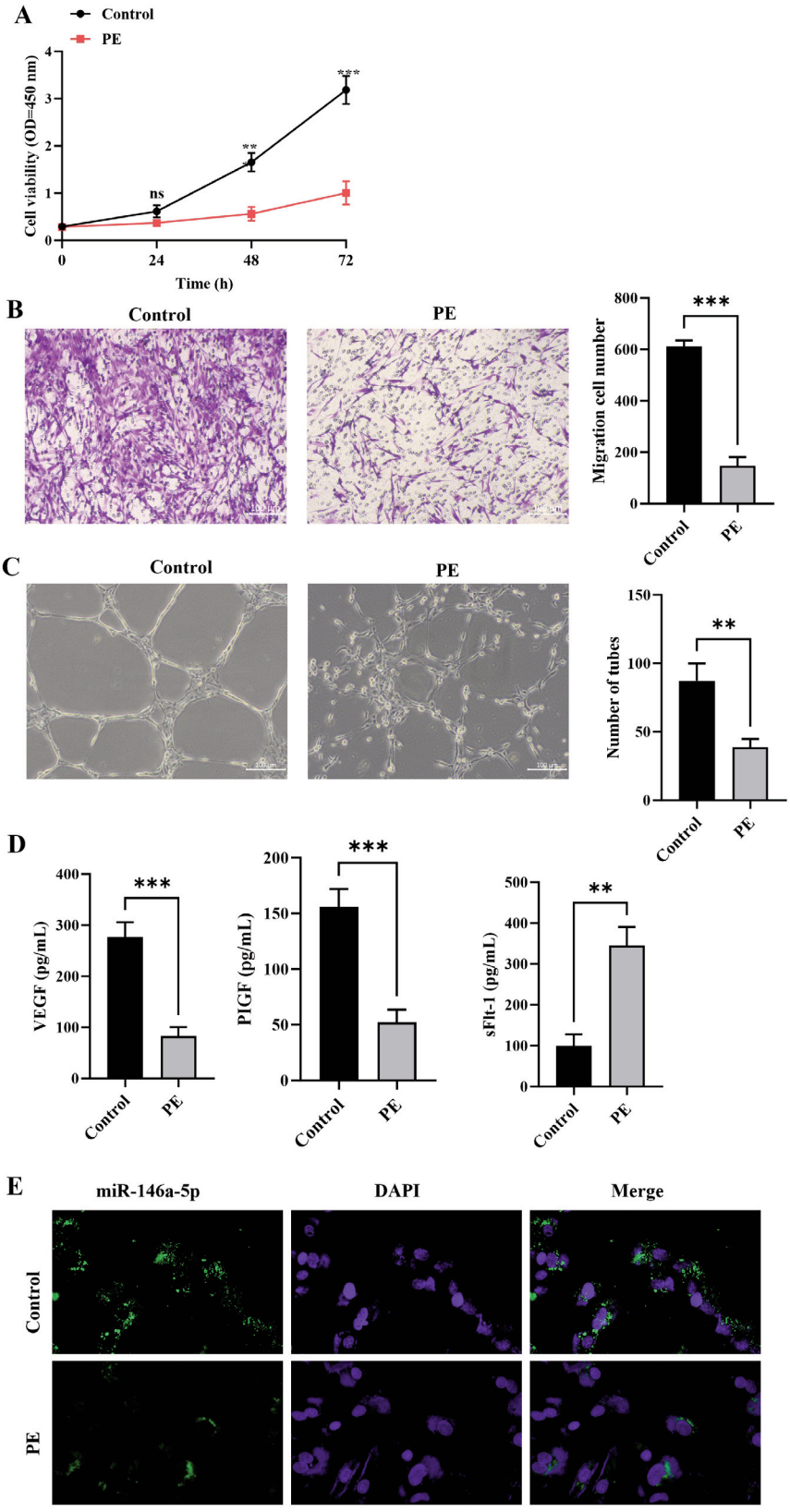

Figure 2. Impaired PMSCs function and downregulated miR-146a-5p expression in preeclampsia patient. **A**) Proliferation of PMSCs measured by CCK-8 assay. **B**) Migration capacity assessed by transwell assay; scale bar:100 μm. (**C**) Angiogenic potential evaluated via tube formation assay; scale bar: 100 μm. **D**) Secretion levels of VEGF, PIGF, and sFlt-1 in PMSC supernatant detected by ELISA. **E**) Localization and expression intensity of *miR-146a-5p* in PMSCs visualized by FISH. Data are presented as mean ±SD (n=3); $^{**}p<0.01$; $^{***}p<0.001$.

hypoxia significantly reduced intracellular *miR-146a-5p* expression, while intervention with either exosomes or *miR-146a-5p* mimic restored its expression level (Figure 3C). Functional rescue assays revealed that hypoxia markedly decreased cell viability (Figure 3D), increased apoptosis rate (Figure 3E), and severely impaired migration capacity (Figure 3F). However, treatment with PMSC-derived exosomes significantly improved cell viability, reduced apoptosis, and restored migration ability. Notably, transfection with *miR-146a-5p* mimic replicated the protective effects of exosomes, substantially reversing hypoxia-induced suppression of viability, increase in apoptosis, and impairment of migration. These results indicate that PMSC-derived exosomes may effectively ameliorate trophoblast cell function under hypoxia-induced injury *via* delivery of *miR-146a-5p*.

Exosomes drive macrophage polarization toward the M2 anti-inflammatory phenotype *via* miR-146a-5p

To investigate the regulatory role of PMSC-derived exosomes on macrophage polarization, human monocytic THP-1 cells were first differentiated into M0 macrophages using PMA induction, followed by stimulation with LPS and IFN-γ to establish an M1 pro-inflammatory macrophage model. RT-qPCR analysis revealed that LPS stimulation significantly downregulated *miR-146a-5p* expression, while intervention with either PMSC-derived exosomes or *miR-146a-5p* mimic effectively restored its expression level (Figure 4A). Flow cytometric analysis of M1/M2 surface markers demonstrated that LPS stimulation markedly increased the expression of M1 marker CD86 and decreased M2 marker CD206.

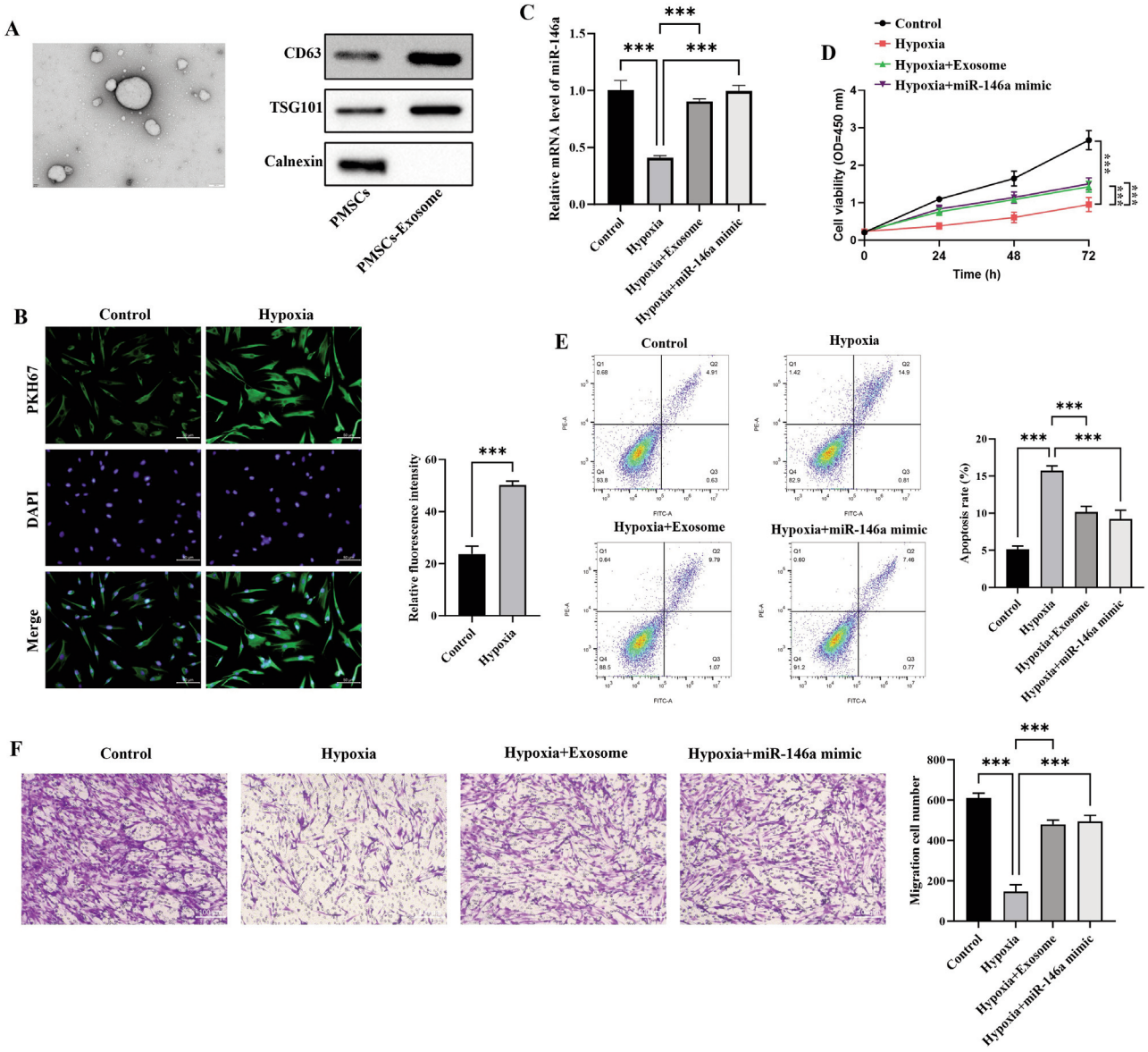

Figure 3. PMSC-derived exosomes improve trophoblast function under hypoxia *via* miR-146a-5p. **A**) Characterization of PMSC-derived exosomes; scale bar: 200 μm. **B**) Internalization of PKH67-labeled exosomes; scale bar: 50 μm. **C**) *miR-146a-5p* expression measured by RT-qPCR. **D**) Cell viability assessed with CCK-8 assay. **E**) Apoptosis rate detected by flow cytometry. **F**) Cell migration ability evaluated *via* transwell assay. Data are presented as mean ±SD (n=3); ***$p<0.001$.

In contrast, treatment with exosomes substantially reversed this polarization imbalance, showing reduced CD86 and elevated CD206 expression (Figure 4B). ELISA further confirmed that exosomes not only significantly suppressed LPS-induced secretion of the pro-inflammatory cytokine TNF-α but also enhanced the production of the anti-inflammatory cytokine IL-10 (Figure 4C). Notably, transfection with *miR-146a-5p* mimic replicated the immunomodulatory effects of exosomes, similarly inhibiting CD86 expression, promoting CD206 expression, reducing TNF-α secretion, and increasing IL-10 secretion. These findings collectively indicate that PMSC-derived exosomes may drive macrophage polarization from the M1 pro-inflammatory phenotype toward the M2 anti-inflammatory phenotype through the delivery of *miR-146a-5p*.

Exosomes promote macrophage M2 polarization and ameliorate placental dysfunction in a PE animal model *via* miR-146a-5p

A PE mouse model was successfully established *via* intraperitoneal injection of L-NAME. The L-NAME group exhibited significantly elevated systolic blood pressure, increased 24 h urinary protein excretion, and fetal growth restriction. Intervention through tail vein injection of either PMSC-derived exosomes or *miR-146a-5p* mimic markedly ameliorated these pathological phenotypes, as evidenced by reduced systolic pressure, decreased urinary protein levels, and restoration of fetal weight to near-normal levels (Figure 5 A-C). Further molecular analysis revealed that the treatment groups showed significantly upregulated expression of angiogenic factors VEGF and PIGF in placental tissues (Figure 5D), accompanied by reduced secretion of the pro-inflammatory cytokine TNF-α and increased secretion of the anti-inflammatory cytokine IL-10 (Figure 5E). Additionally, evaluation of macrophage polarization markers demonstrated elevated mRNA expression of the M2 marker *Arg1* and decreased expression of the M1 marker *iNOS* (Figure 5F). These findings collectively indicate that exosomes may effectively reverse L-NAME-induced placental dysfunction *via* delivery of *miR-146a-5p*, with the therapeutic effects being closely associated with improved angiogenesis, suppressed inflammatory response, and promotion of macrophage polarization toward the M2 anti-inflammatory phenotype.

miR-146a-5p targets and inhibits the TRAF6/NF-κB pathway to ameliorate PE

To elucidate the molecular mechanism by which *miR-146a-5p* regulates the pathological process of PE, a dual luciferase reporter assay was first performed to validate its targeting relationship with

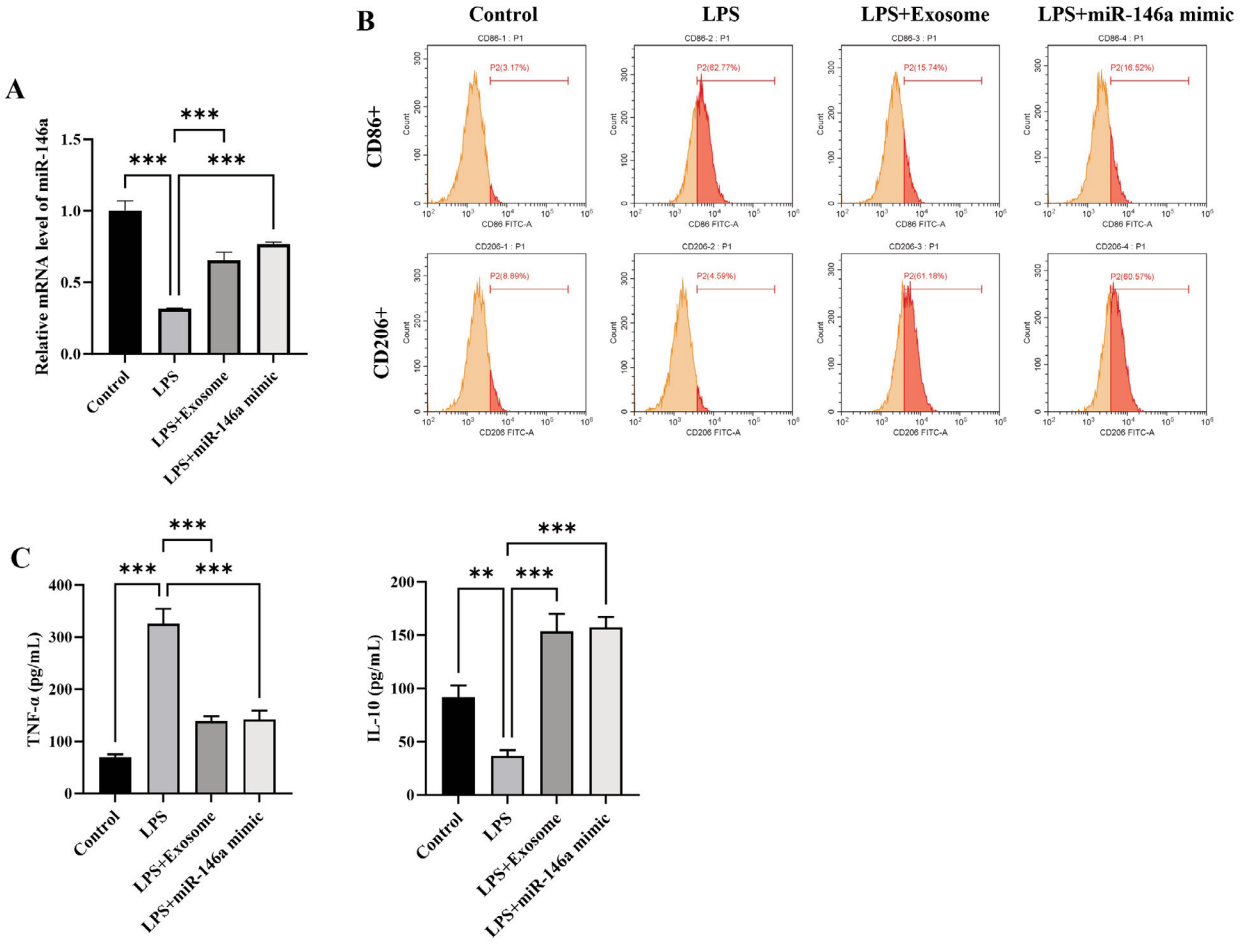

Figure 4. Exosomes promote macrophage M2 polarization and ameliorate placental dysfunction in a preeclampsia animal model *via* miR-146a-5p. **A**) Expression of *miR-146a-5p* in macrophages measured by RT-qPCR. **B**) Flow cytometry analysis of M1/M2 surface markers in macrophages. **C**) Secretion levels of TNF-α and IL-10 in macrophage supernatant detected by ELISA. Data are presented as mean ± SD (n=3); ***p*<0.01; ****p*<0.001.

TRAF6. Using the TargetScan database, we predicted binding sites between *miR-146a-5p* and the 3'-UTR of *TRAF6* mRNA (Figure 6A). Co-transfection of the wild-type *TRAF6* luciferase reporter vector (*WT-TRAF6*) with *miR-146a-5p* mimic significantly reduced luciferase activity, while no change was observed in the mutant vector (*MUT-TRAF6*) transfection group (Figure 6B), confirming that *miR-146a-5p* directly binds to and targets *TRAF6* mRNA. Western blot analysis further demonstrated that both exosomes and *miR-146a-5p* mimic markedly suppressed the expression of TRAF6 and phosphorylated NF-κB (p-NF-κB) in both macrophages and trophoblast cells, an effect that was reversible upon treatment with a *miR-146a-5p* inhibitor. In hypoxia-induced HTR-8/SVneo cells, the expression of TRAF6 and p-NF-κB was significantly elevated; intervention with either exosomes or *miR-146a-5p* mimic reduced their expression, while transfection with miR-146a-5p inhibitor restored protein levels (Figure 6C). A consistent regulatory pattern was observed in an LPS-stimulated THP-1 macrophage model: the L-NAME group exhibited abnormally high expression of TRAF6 and p-NF-κB, which was significantly downregulated by exosome or mimic treatment, and partially restored upon inhibitor intervention (Figure 6D). These results collectively demonstrate that *miR-146a-5p* directly targets *TRAF6* mRNA to inhibit its expression, thereby blocking the activation of the NF-κB signaling pathway. This mechanism constitutes the molecular basis through which exosomes ameliorate inflammatory injury in PE.

Discussion

PE is a severe gestational disorder whose core pathology involves placental dysfunction leading to systemic vascular endothelial injury and disruption of the immune microenvironment.[22] This study demonstrates for the first time that exosomes derived from PMSCs restore trophoblast function and reverse imbalance in macrophage polarization *via* delivery of *miR-146a-5p*. This dual regulatory effect ultimately ameliorates pathological phenotypes in animal models by suppressing the TRAF6/NF-κB signaling pathway, providing a novel therapeutic strategy for PE treatment. Macrophage polarization, particularly the M1/M2 balance, serves as a central regulatory hub within the placental immune microenvironment and plays a pivotal role in the pathogenesis of PE.[3,23,24] Substantial evidence indicates that a shift toward the pro-inflammatory M1 phenotype, characterized by high expression of CD86 and secretion of cytokines such as TNF-α and IL-6, disrupts placental function by directly damaging trophoblast cells and impairing angiogenesis, thereby exacerbating placental hypoxia and maternal systemic inflammatory responses.[4,25] Notably, exosomes derived from MSCs and their carried specific *miRNAs* have been demonstrated to effectively modulate macrophage polarization in various disease models; for instance, the delivery of anti-inflammatory *miRNAs* can promote a transition toward the reparative M2 phenotype.[26,27] However, the specific

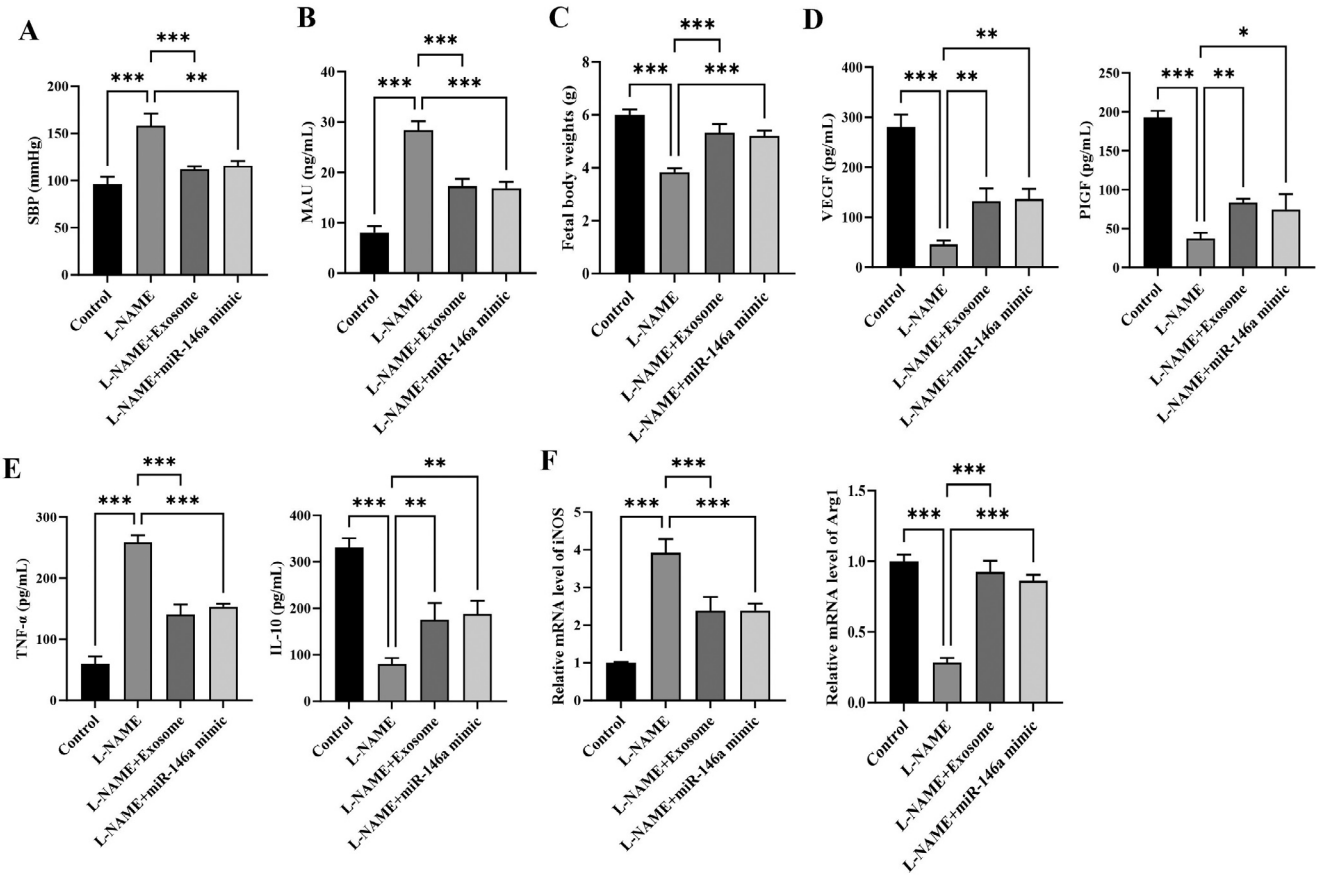

Figure 5. Exosomes promote macrophage M2 polarization and ameliorate placental dysfunction in a preeclampsia animal model *via* miR-146a-5p. **A**) Systolic blood pressure in mice (n=5). **B**) 24 h microalbuminuria levels (n=5). **C**) Fetal weight measurements (n=5). **D**) VEGF and PIGF levels in placental tissue measured by ELISA (n=3). **E**) Serum levels of TNF-α and IL-10 detected by ELISA (n=3). **F**) mRNA expression of *Arg1* and *iNOS* in placental tissue analyzed by RT-qPCR (n=3). Data are presented as mean ±SD; *p<0.05; **p<0.01; ***p<0.001.

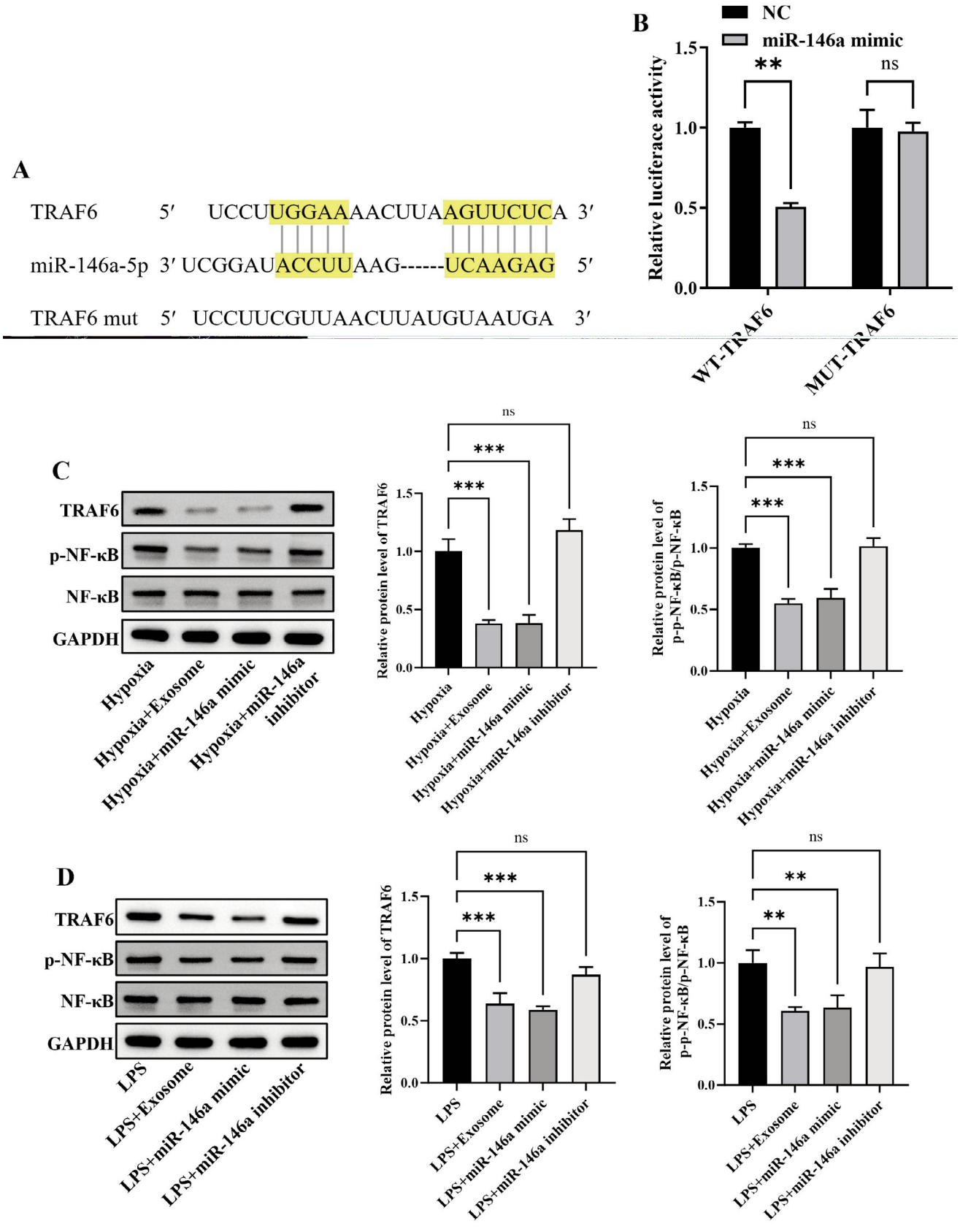

Figure 6. miR-146a-5p ameliorates preeclampsia by targeting TRAF6/NF-κB pathway. **A**) The binding sites between *miR-146a* and *TRAF6* were predicted via the TargetScan database. **B**) Dual luciferase reporter assay. **C**) Western blot analysis of TRAF6, p-NF-κB, and NF-κB protein expression in HTR-8/SVneo cells. **D**) Western blot analysis of TRAF6, p-NF-κB, and NF-κB protein expression in THP-1 cells. Data are presented as mean ±SD (n=3); ns, $p>0.05$; **$p<0.01$; ***$p<0.001$.

regulatory role of a key effector *miRNA*, *miR-146a-5p*, delivered by exosomes in the context of PE, particularly concerning its impact on macrophage polarization and its association with trophoblast dysfunction, remains a significant knowledge gap. This study is the first to systematically validate the corrective effect of PMSC-derived exosomes and their delivered *miR-146a-5p* on the imbalance of macrophage polarization in a PE model. This finding provides a novel molecular basis for developing cell-free therapeutic strategies that target the placental immune microenvironment and simultaneously restore the impaired crosstalk between trophoblasts and macrophages.

Substantial evidence indicates that aberrant activation of the NF-κB signaling pathway serves as a central mechanism driving multiple core pathological features of PE.[28,29] *TRAF6*, a key upstream regulator of this pathway, functions as a critical molecular switch that triggers inflammatory cascades by modulating IKK complex activity, subsequent IκB degradation, and nuclear translocation of NF-κB.[30] Activation of the TRAF6/NF-κB axis has been demonstrated to promote pro-inflammatory M1 macrophage polarization and tissue damage in various disease models, including PE.[31,32] Notably, *miR-146a-5p* acts as an important negative feedback regulator of NF-κB signaling by directly targeting the 3' UTR of *TRAF6* mRNA to suppress its expression, thereby effectively inhibiting downstream NF-κB activation.[33] This regulatory mechanism has been shown to mitigate inflammatory injury and modulate immune cell function in models of acute pancreatitis and arthritis.[34,35] However, within the context of PE, direct evidence remains scarce regarding whether and how *miR-146a-5p* coordinates the regulation of both macrophage polarization homeostasis and trophoblast function through targeted suppression of the TRAF6/NF-κB pathway. This study provides the first demonstration in a PE model that *miR-146a-5p*, delivered by PMSC-derived exosomes, directly targets and inhibits *TRAF6* expression, thereby effectively suppressing NF-κB pathway activation. Elucidation of this mechanism not only explains the pathway underlying the exosome-mediated therapeutic effects but also establishes the miR-146a-5p/TRAF6/NF-κB axis as a key regulatory hub linking placental immune microenvironment dysregulation and trophoblast impairment, offering a solid molecular basis for developing cell-free therapies targeting this axis.

Angiogenesis is a critical process in embryonic development and tissue repair, maintaining a delicate equilibrium through the coordinated actions of pro-angiogenic factors (*VEGF*, *PIGF*) and anti-angiogenic factors (*sFlt-1*).[36] In pathological contexts such as cancer, pro-angiogenic signaling is often upregulated, facilitating rapid tumor growth by enhancing nutrient supply.[37] In contrast, PE, a pregnancy-specific disorder, is characterized by a distinct shift toward an anti-angiogenic state.[38,39] This condition is predominantly characterized by a significant elevation of *sFlt-1* in placental tissue. Functioning as a decoy receptor, *sFlt-1* potently binds and neutralizes the biological activities of *VEGF* and *PIGF*, leading to systemic vascular endothelial dysfunction and subsequent clinical manifestations of PE, including hypertension and proteinuria.[40] Notably, the transcription factor NF-κB plays a complex role in modulating angiogenic equilibrium. Evidence suggests that NF-κB activation promotes *sFlt-1* production, thereby inhibiting VEGF/PIGF signaling,[41] a mechanism that may crucially underlie the dysregulated angiogenesis observed in preeclampsia. This mechanism may be central to the dysregulated angiogenesis characteristic of PE.

Although this study elucidates the synergistic mechanism by which PMSCs-derived exosomes ameliorate PE *via* the miR-146a-5p/TRAF6 axis, several limitations must be acknowledged. First, while we observed functional recovery in both trophoblasts and macrophages, it remains unclear whether the administered exosomes were equally taken up by all cell types in the placental microenvironment or exhibited a preferential targeting for dysfunctional cells. Second, the absence of CRISPR/Cas9-mediated knockout of *miR-146a-5p* in PMSCs makes it difficult to fully exclude the potential contribution of other miRNAs involved in the observed effects. Furthermore, the animal models did not evaluate the long-term biosafety profile of exosome administration or its impact on offspring development. Furthermore, the low yield of exosomes prepared using ultracentrifugation presents a major challenge for large-scale production and clinical application. Finally, the optimal therapeutic window, dosage regimen, and frequency of administration require systematic investigation in future studies.

In summary, this study systematically elucidates the central mechanism by which PMSC-derived exosomes orchestrate the improvement of trophoblast-immune microenvironment interactions *via* the miR-146a-5p/TRAF6/NF-κB axis. Specifically, exosome-delivered *miR-146a-5p* targets and suppresses *TRAF6* expression, leading to significant inhibition of the NF-κB-mediated inflammatory cascade and directly driving the shift in macrophage polarization from the pro-inflammatory M1 phenotype toward the reparative M2 phenotype. This remodeling of the polarization state represents a crucial step in reversing placental immune microenvironment dysregulation. These findings not only provide a novel direction for developing targeted therapies for PE but also offer a theoretical framework for immune microenvironment intervention strategies in other pregnancy-related disorders.

References

1. Mol BWJ, Roberts CT, Thangaratinam S, Magee LA, de Groot CJM, Hofmeyr GJ. Pre-eclampsia. Lancet 2016;387:999-1011.
2. Phipps EA, Thadhani R, Benzing T, Karumanchi SA. Pre-eclampsia: pathogenesis, novel diagnostics and therapies. Nat Rev Nephrol 2019;15:275-89.
3. Deer E, Herrock O, Campbell N, Cornelius D, Fitzgerald S, Amaral LM, et al. The role of immune cells and mediators in preeclampsia. Nat Rev Nephrol 2023;19:257-70.
4. Wei Y, Su Y, Liu C, Ma X, Ling Z, Wang Y, et al. Macrophage and preeclampsia: macrophage polarization imbalance at the maternal-fetal interface. J Clin Lab Anal 2025;39:e70046.
5. Liu X, Fei H, Yang C, Wang J, Zhu X, Yang A, et al. Trophoblast-derived extracellular vesicles promote preeclampsia by regulating macrophage polarization. Hypertension 2022;79:2274-87.
6. Wang Y, Fang J, Liu B, Shao C, Shi Y. Reciprocal regulation of mesenchymal stem cells and immune responses. Cell Stem Cell 2022;29:1515-30.
7. Liu H, Zhang X, Zhang M, Zhang S, Li J, Zhang Y, et al. Mesenchymal stem cell derived exosomes repair uterine injury by targeting transforming growth factor-beta signaling. ACS Nano 2024;18:3509-19.
8. Hade MD, Suire CN, Suo Z. Mesenchymal Stem cell-derived exosomes: applications in regenerative medicine. Cells 2021;10:1959.
9. Arabpour M, Saghazadeh A, Rezaei N. Anti-inflammatory and M2 macrophage polarization-promoting effect of mesenchymal stem cell-derived exosomes. Int Immunopharmacol 2021;97:107823.
10. Krylova SV, Feng D. The machinery of exosomes: biogenesis, release, and uptake. Int J Mol Sci 2023;24:1337.
11. Isaac R, Reis FCG, Ying W, Olefsky JM. Exosomes as mediators of intercellular crosstalk in metabolism. Cell Metab 2021;33:1744-62.
12. Rahimian N, Nahand JS, Hamblin MR, Mirzaei H. Exosomal MicroRNA profiling. Methods Mol Biol 2023;2595:13-47.

13. Rao A, Shinde U, Das DK, Balasinor N, Madan T. Early prediction of pre-eclampsia using circulating placental exosomes: Newer insights. Indian J Med Res 2023;158:385-96.
14. Wang Y, Li B, Zhao Y. Inflammation in preeclampsia: genetic biomarkers, mechanisms, and therapeutic strategies. Front Immunol 2022;13:883404.
15. Zhang H, He Y, Wang JX, Chen MH, Xu JJ, Jiang MH, et al. miR-30-5p-mediated ferroptosis of trophoblasts is implicated in the pathogenesis of preeclampsia. Redox Biol 2020;29:101402.
16. Jaszczuk I, Koczkodaj D, Kondracka A, Kwasniewska A, Winkler I, Filip A. The role of miRNA-210 in pre-eclampsia development. Ann Med 2022;54:1350-6.
17. Chen J, Chen J, Li Q, Hu M, Zhong X, Yu L, et al. Astragaloside promotes the secretion of MSC-derived exosomal miR-146a-5p by regulating TRAF6/NF-kappaB pathway to attenuate inflammation in high glucose-impaired endothelial cells. In Vitro Cell Dev Biol Anim 2025;61:93-106.
18. Qin M, Wang Y, Wang Z, Dong B, Yang P, Liu Y, et al. Adipose-derived small extracellular vesicle miR-146a-5p targets Fbx32 to regulate mitochondrial autophagy and delay aging in skeletal muscle. J Nanobiotechnol 2025;23:287.
19. Zisman D, Safieh M, Simanovich E, Feld J, Kinarty A, Zisman L, et al. Tocilizumab (TCZ) Decreases angiogenesis in rheumatoid arthritis through its regulatory effect on miR-146a-5p and EMMPRIN/CD147. Front Immunol 2021;12:739592.
20. Liu C, Xue J, Xu B, Zhang A, Qin L, Liu J, et al. Exosomes derived from miR-146a-5p-Enriched mesenchymal stem cells protect the cardiomyocytes and myocardial tissues in the polymicrobial sepsis through regulating MYBL1. Stem Cells Int 2021;2021:1530445.
21. Iacona JR, Lutz CS. miR-146a-5p: Expression, regulation, and functions in cancer. Wiley Interdiscip Rev RNA 2019;10:e1533.
22. Opichka MA, Rappelt MW, Gutterman DD, Grobe JL, McIntosh JJ. Vascular dysfunction in preeclampsia. Cells 2021;10:3055.
23. Yao Y, Xu XH, Jin L. Macrophage polarization in physiological and pathological pregnancy. Front Immunol 2019;10:792.
24. Hutter S, Heublein S, Knabl J, Andergassen U, Vrekoussis T, Makrigiannakis A, et al. Macrophages: are they involved in endometriosis, abortion and preeclampsia and how? J Nippon Med Sch 2013;80:97-103.
25. Vishnyakova P, Elchaninov A, Fatkhudinov T, Sukhikh G. Role of the monocyte-macrophage system in normal pregnancy and preeclampsia. Int J Mol Sci 2019;20:3695.
26. Harrell CR, Jovicic N, Djonov V, Arsenijevic N, Volarevic V. Mesenchymal stem cell-derived exosomes and other extracellular vesicles as new remedies in the therapy of inflammatory diseases. Cells 2019;8:1605.
27. Tian S, Zhou X, Zhang M, Cui L, Li B, Liu Y, et al. Mesenchymal stem cell-derived exosomes protect against liver fibrosis via delivering miR-148a to target KLF6/STAT3 pathway in macrophages. Stem Cell Res Ther 2022;13:330.
28. Shen W, Wang Q, Shen G, Gu M, Shen Q, Zhang A, et al. Regulation of macrophage polarization by metformin through inhibition of TLR4/NF-kappaB pathway to improve pre-eclampsia. Placenta 2025;160:89-99.
29. Jung KY, Uprety LP, Jang YJ, Yang JI. Pro-inflammatory mediators and signaling proteins in the decidua of pre-eclampsia. Eur Rev Med Pharmacol Sci 2020;24:12016-24.
30. Duan Y, Yu C, Kuang W, Li J, Qiu S, Ni S, et al. Mesenchymal stem cell exosomes inhibit nucleus pulposus cell apoptosis via the miR-125b-5p/TRAF6/NF-kappaB pathway axis. Acta Biochim Biophys Sin (Shanghai) 2023;55:1938-49.
31. Xu Y, Liao C, Liu R, Liu J, Chen Z, Zhao H, et al. IRGM promotes glioma M2 macrophage polarization through p62/TRAF6/NF-kappaB pathway mediated IL-8 production. Cell Biol Int 2019;43:125-35.
32. Chang B, Wang Z, Cheng H, Xu T, Chen J, Wu W, et al. Acacetin protects against sepsis-induced acute lung injury by facilitating M2 macrophage polarization via TRAF6/NF-kappaB/COX2 axis. Innate Immun 2024;30:11-20.
33. Sun J, Liao Z, Li Z, Li H, Wu Z, Chen C, et al. Down-regulation miR-146a-5p in Schwann cell-derived exosomes induced macrophage M1 polarization by impairing the inhibition on TRAF6/NF-kappaB pathway after peripheral nerve injury. Exp Neurol 2023;362:114295.
34. Zheng C, Ji Z, Xu Z, Du Z, Wang Z. Overexpression of miR-146a-5p Ameliorates inflammation and autophagy in TLCs-induced AR42J cell model of acute pancreatitis by inhibiting IRAK1/TRAF6/NF-kappaB pathway. Ann Clin Lab Sci 2022;52:416-25.
35. Zhong JH, Li J, Liu CF, Liu N, Bian RX, Zhao SM, et al. Effects of microRNA-146a on the proliferation and apoptosis of human osteoarthritis chondrocytes by targeting TRAF6 through the NF-kappaB signalling pathway. Biosci Rep 2017;37:BSR20160578.
36. Griffioen AW, Dudley AC. The rising impact of angiogenesis research. Angiogenesis 2022;25:435-7.
37. Treps L, Gavard J. [Tumor angiogenesis: when the tree of life turns bad].[Article in French]. Med Sci (Paris) 2015;31:989-95.
38. Verdonk K, Visser W, Steegers EA, Kappers M, Danser AH, van den Meiracker AH. [New insights into the pathogenesis of pre-eclampsia: the role of angiogenesis-inhibiting factors].[Article in Dutch]. Ned Tijdschr Geneeskd 2011;155:A2946.
39. Virtanen A, Huttala O, Tihtonen K, Toimela T, Heinonen T, Uotila J. Angiogenic capacity in pre-eclampsia and uncomplicated pregnancy estimated by assay of angiogenic proteins and an in vitro vasculogenesis/angiogenesis test. Angiogenesis 2019;22:67-74.
40. Wazan LE, Widhibrata A, Liu GS. Soluble FLT-1 in angiogenesis: pathophysiological roles and therapeutic implications. Angiogenesis 2024;27:641-61.
41. Logan MK, Lett KE, McLaurin DM, Hebert MD. Coilin as a regulator of NF-kB mediated inflammation in preeclampsia. Biol Open 2022;11:bio059326.

Received: 29 September 2025. Accepted: 3 November 2025.

Licensee PAGEPress, Italy
European Journal of Histochemistry 2025; 69:4426
doi:10.4081/ejh.2025.4426